Syngas Chemical Looping Process: Dynamic Modeling of a Moving-Bed Reducer

Qiang Zhou, Liang Zeng, and Liang-Shih Fan
Dept. of Chemical and Biomolecular Engineering, The Ohio State University, Columbus, OH 43210

DOI 10.1002/aic.14181
Published online August 5, 2013 in Wiley Online Library (wileyonlinelibrary.com)

The syngas chemical looping process coproduces hydrogen and electricity with iron oxide based oxygen carriers in a circulating moving bed system. In this article, a one-dimensional (1-D) dynamic model is developed to simulate the countercurrent gas–solid reactive flow in the moving-bed reducer. This model is validated by TGA and bench-scale experiments. Both the steady state and dynamic composition profiles are obtained to help understand the reaction and reactor behaviors. Numerical simulation on the effects of reactor length is conducted to optimize the moving-bed reducer design. It is also found that minor variations in the feed rate ratio near a critical point that is represented by the reaction equilibrium could yield a significant difference in the time required for the reactions to reach a steady-state operation. Such a difference has an important practical implication in that the moving-bed reducer should be designed and operated to circumvent the critical point. © 2013 American Institute of Chemical Engineers *AIChE J*, 59: 3432-3443, 2013

Keywords: reaction kinetics, mathematical modeling, reactor analysis

Introduction

Chemical looping technology for fossil fuel conversion is an increasing field of interest as global concerns for CO_2 emissions escalation.[1,2] The unique feature of this novel technology is in its significantly high-fuel processing efficiency and versatility with near 100% CO_2 capture. Specifically, chemical looping processes utilize the reduction-oxidation (redox) cycles of metal oxide composites, or namely oxygen carrier (OC) particles. In the oxygen carrier reduction step, fuel is fully converted to CO_2 and H_2O, where H_2O can be easily condensed out, resulting in a high-purity CO_2 stream for geological sequestration or enhanced oil recovery. The reactor is named as the reducer or fuel reactor. In the oxidation step, the oxygen carrier particles are regenerated by steam/air while producing H_2/heat. This reactor is called the oxidizer/combustor or steam/air reactor. As shown in Figure 1, the chemical looping scheme avoids direct carbonaceous fuel mixing with oxidants, which prevents the costly separation of a gaseous mixture of CO_2 and H_2/N_2. For conventional combustion and gasification approaches, CO_2 separation and compression will inevitably impose a 20–30% parasitic energy penalty relative to plants without carbon emission control.[3,4] In comparison, the chemical looping process only has a 3–5% energy penalty, which translates into a significant potential cost advantage when compared to conventional CO_2 capture technologies. Additionally, chemical looping technology can be adopted to produce electricity, hydrogen, and/or syngas for liquid fuel and chemical synthesis.[4]

The oxygen carrier particles undergo cyclic redox cycles, and their physical and chemical properties play a vital role in the chemical looping system. Hundreds of metal oxide compositions have been synthesized and tested.[5] Among them, iron oxide is considered as one of the most promising, primary metal oxides due to its favorable thermodynamic property, low-raw material cost, high-oxygen carrying capacity, high-melting points, good mechanical strength, and small environmental and health concerns. The redox reactions of the iron based oxygen carrier particles involve hematite (Fe_2O_3), magnetite (Fe_3O_4), wustite (Fe_xO, $0.830<x<0.952$), and metallic iron (Fe). A comprehensive understanding on the thermodynamics and kinetics between each phase and the fuel is needed for the overall system design. It is noted that for the reducer operation, Fe_2O_3 is capable of fully oxidizing fuel to CO_2 and H_2O, whereas Fe_3O_4 and Fe_xO can only partially oxidize fuel into a mixture of CO, CO_2, H_2 and H_2O.[6] Mattisson et al. conducted redox experiments between Fe_2O_3 to Fe_3O_4 and showed that the reaction rates depend on the support used.[7] Li et al. synthesized an iron based composite oxygen carrier particle, which is 10 times more reactive than commercially available iron oxide and can sustain more than 100 redox cycles, according to thermogravimetric analysis (TGA) tests.[8] These achievements on oxygen carrier particles have established a solid foundation for further chemical looping process development.

In addition to the oxygen carrier material development, reactor design is another key factor influencing the success of chemical looping technology. Most chemical looping processes are developed based on an interconnected fluidized bed design, which is characterized by a mixed gas and solid

Correspondence concerning this article should be addressed to L-S. Fan at. fan@chbmeng.ohio-state.edu.

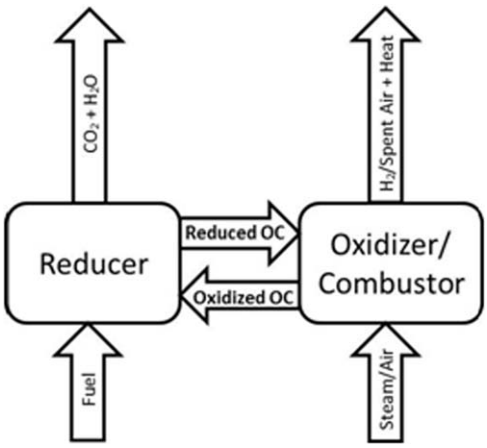

Figure 1. General chemical looping scheme.

flow in all the reactors.[9–13] The air oxidation reaction in a fluidized-bed combustor is intrinsically fast and is thermodynamically favored. The mixed flow pattern in the reducer, however, only allows Fe_2O_3 to be reduced to Fe_3O_4 for a complete fuel conversion.[6] Alternatively, a countercurrent gas–solid contacting pattern in the reducer could create multiple equilibrium stages along the reactor. The top equilibrium stage can ensure that the fuel is fully converted under an oxidizing environment where Fe_2O_3 is introduced. The bottom equilibrium stage can help further reduce the iron oxide to Fe/Fe_xO under a reducing environment where fuel is injected. Such countercurrent flow patterns can be obtained in a moving, dense packed bed, or multistage fluidized bed. Previous thermodynamic modeling results show that in order to achieve 10% fuel conversion, the maximum iron oxide conversions in a well-mixed flow versus a countercurrent flow are 11.1% (equivalent to Fe_3O_4) and >50% (equivalent to a mixture of Fe_xO/Fe), respectively.[6] Thus, for a given capacity of a reactor system, a moving bed or a multistage fluidized-bed reducer requires a significantly lower oxygen carrier circulation rate than does a fluidized-bed reducer.

Based on the concept discussed earlier, a syngas chemical looping (SCL) process has been developed.[2] The SCL process circulates iron-based oxygen carrier particles through three reactors for hydrogen and electricity coproduction while using syngas as a fuel and capturing CO_2. The syngas is mainly composed of CO and H_2 and is derived from a typical coal or biomass oxygen blown gasifier. The SCL reducer is a good example of a countercurrent moving-bed operation, which ensures for the full conversion of fuels while enhancing the extent of iron based oxygen carrier conversion. The high extent of conversion of the iron based oxygen carrier facilitates the generation of hydrogen from steam-iron reaction in the oxidizer. The combustor fully regenerates the oxygen carrier particles, which are then circulated back to the reducer via a riser. Table 1 summarizes all the key reactions involved in the SCL process. The SCL moving-bed reducer concept and application have been proven in a bench scale unit,[6] and the SCL integrated process has been tested under a 25kWth subpilot scale continuous operation for more than 300 h.[14,15] In order to further scale-up the chemical looping process, issues such as cost, time, safety, and other uncertainties in larger unit operations need to be examined. To address these uncertainties, advanced reactor modeling is highly desired and the modeling efforts can accelerate the SCL technology development, reduce the pilot-scale facility design time and operating campaigns, as well as reduce the cost and technical risks.

The countercurrent moving bed operation is seen in many industrial applications such as blast furnaces, kiln heaters, and adsorptions. Professor Neal Amundson was the pioneer in the mathematical modeling and analysis of the moving bed systems and made monumental contributions to the fundamental understanding of the behavior of these systems.[16–18] This article is, thus, a fitting tribute to him, particularly in light of his specific contributions to this subject. Previous computational efforts on chemical looping process development have heavily focused on fluidized-bed reducer modeling and analysis, which was recently reviewed by Adanez et al.[19] Kang et al. developed a steady-state model for a countercurrent moving bed reducer.[20] A one-step reduction from Fe_2O_3 to Fe_xO was assumed in their model, which is unrealistic and, thus, does not represent the complex rate process of this reaction system.[21,22] Additionally, many of the earlier modeling work lacks first-hand experimental data for comparisons and validation. This work, however, does compare numerical results with experimental results. An effective moving bed reducer model should consider the reaction kinetic rate and thermodynamic equilibrium between the gas mixture and iron oxides in the context of the gas solid countercurrent flow system. In this work, a 1-D dynamic reactive flow model is developed to simulate the countercurrent gas–solid interaction within a moving bed reducer in the SCL process. A three-interface shrinking core model is used to represent the overall reaction thermodynamics and kinetics of individual iron based oxygen carrier particles. The individual particle model is validated by experimental TGA data. The 1-D moving bed code is validated by comparing the modeling results with the experimental data from a 2.5 kW_{th} bench-scale reactor that the authors obtained earlier. The model is used to investigate the flow and reaction progress and assist in the design and optimization of the SCL reducer.

Mathematical Model

Oxygen carrier kinetic model

Turkdogan et al. systematically studied the reduction of iron ores of different sizes at various operating conditions of temperatures and gas compositions.[21–23] They found that the rate-limiting step varies from reaction control (Fe_2O_3-Fe_3O_4 reduction) to diffusion control (Fe_3O_4-Fe_xO—Fe reduction). To study the iron oxide reduction kinetics, various models have been developed in the literature such as the shrinking core model, cracking core model, particle-pellet (grain) model, and nucleation and growth model. De Lasa briefly

Table 1. Key Reactions in the SCL Process

Reactor	Reactions
Reducer	$3Fe_2O_3 + CO/H_2 = 2Fe_3O_4 + CO_2/H_2O$
	$(x/(4x-3))Fe_3O_4 + CO/H_2 = (3/(4x-3))$ $Fe_xO + CO_2/H_2O$
	$Fe_xO + CO/H_2 = xFe + CO_2/H_2O$
Oxidizer	$xFe + H_2O = Fe_xO + H_2$
	$(3/(4x-3))Fe_xO + H_2O = (x/(4x-3))$ $Fe_3O_4 + H_2$
Combustor	$4Fe_3O_4 + O_2 = 6Fe_2O_3$

reviewed these models and their applications in chemical looping reaction systems.[24]

The shrinking core model is used in this study to consider the oxygen carrier reaction thermodynamics and kinetics. The unreacted shrinking core model (USCM) is commonly used to describe the reaction of gas–solid reaction systems.[25] It considers three major factors that affect the overall reaction rate, that is, diffusion through the gas film, intraparticle diffusion, and surficial chemical reaction at reaction interface. The USCM model is valid based on the following assumptions: first, the interfacial chemical reaction is a first-order reversible chemical reaction; [25] second, isothermal and isobaric conditions are throughout the particle; and third, the volume of a pellet is unchanged with the progress of the reaction. Because the heat of the reaction between syngas and iron oxides is nearly zero and the current reactor system includes heaters to give isothermal operation, the second assumption is met. The last assumption only applies to certain composite iron oxide material. Pure iron oxide reduction is a particle volume increasing process due to the dominating outward diffusion of the iron ion. The oxygen carrier particles used in the SCL process are supported iron oxide materials, and the support material could enhance the oxygen vacancy diffusivity, and, thus, limit the volume change.[4,8] In order to determine the reaction rate and the time for complete conversion, a three-interface USCM is adopted to represent the three reactions in the reducer as listed in Table 1 (also can be found are Reactions 4–6).[26] It is noted that

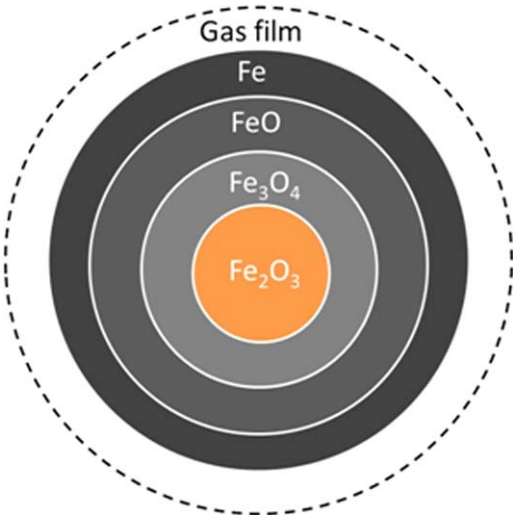

Figure 2. Schematic diagram of the unreacted shrinking core model.

[Color figure can be viewed in the online issue, which is available at wileyonlinelibrary.com.]

$Fe_{0.952}O$ in this current model is used to represent the wustite phase. The three-interface USCM is illustrated in Figure 2, and reaction rates in each reaction step are obtained through the following expressions

$$V_1=\frac{P}{\tilde{R}T\omega}\left\{\begin{array}{l}A_3(A_2+B_2+B_3+F)+(A_2+B_2)(B_3+F)(y-y_1{}^*)\\-[A_3(B_2+B_3+F)+B_2(B_3+F)](y-y_2{}^*)-A_2(B_3+F)(y-y_3{}^*)\end{array}\right\} \tag{1}$$

$$V_2=\frac{P}{\tilde{R}T\omega}\left\{\begin{array}{l}[(A_1+B_1+B_2)(A_3+B_3+F)+A_3(B_3+F)](y-y_2{}^*)\\-[B_2(A_3+B_3+F)+A_3(B_3+F)](y-y_1{}^*)-(A_1+B_1)(B_3+F)(y-y_3{}^*)\end{array}\right\} \tag{2}$$

$$V_3=\frac{P}{\tilde{R}T\omega}\left\{\begin{array}{l}[(A_1+B_1)(A_2+B_2+B_3+F)+A_2(B_2+B_3+F)](y-y_3{}^*)\\-A_2(B_3+F)](y-y_1{}^*)-(A_1+B_1)(B_3+F)(y-y_2{}^*)\end{array}\right\} \tag{3}$$

where

$$A_1=\frac{1}{(1-R_M)^{2/3}}\frac{1}{k_1(1+1/K_1)} \tag{4}$$

$$A_2=\frac{1}{(1-R_W)^{2/3}}\frac{1}{k_2(1+1/K_2)} \tag{5}$$

$$A_3=\frac{1}{(1-R_F)^{2/3}}\frac{1}{k_3(1+1/K_3)} \tag{6}$$

$$B_1=\frac{(1-R_W)^{1/3}-(1-R_M)^{1/3}}{(1-R_M)^{1/3}(1-R_W)^{1/3}}\frac{d_p}{2D_1} \tag{7}$$

$$B_2=\frac{(1-R_F)^{1/3}-(1-R_W)^{1/3}}{(1-R_W)^{1/3}(1-R_F)^{1/3}}\frac{d_p}{2D_2} \tag{8}$$

$$B_3=\frac{1-(1-R_F)^{1/3}}{(1-R_F)^{1/3}}\frac{d_p}{2D_3} \tag{9}$$

$$F=1/k_f \tag{10}$$

$$\begin{aligned}\omega=&(A_1+B_1)[A_3(A_2+B_2+B_3+F)+(A_2+B_2)(B_3+F)]\\&+A_2[A_3(B_2+B_3+F)+B_2(B_3+F)]\end{aligned} \tag{11}$$

It is noted that, in the reducer, all the three reactions might not take place concurrently. There may be only one or two reactions proceeding in a certain period of time. Under these circumstances, the reaction rate must be calculated through formula for the states of two interfaces or a single interface reacting.[26] The overall fraction of reduction of iron oxide particles can be expressed as follows based on the chemical formula of reduction products

$$R=0.1111R_M+0.1889R_W+0.7R_F \tag{12}$$

where R_M, R_W, R_F, correspond to the conversions from Fe_2O_3 to Fe_3O_4, Fe_3O_4 to Fe_xO, and Fe_xO to Fe, respectively. In addition, the water-gas shift reaction in the gas phase is considered in this work. The reaction rate and equilibrium constant of the water gas shift reaction are based on the formulas in the literature.[26,27]

One-dimensional (1-D) model for the moving-bed reducer

In order to simulate the moving-bed reducer in the SCL process accurately, a suitable flow model is highly needed to describe the gas and solid flow pattern within the reactor. There are various flow models that can be employed. In this article, a 1-D flow model is developed to simulate the countercurrent gas–solid flow pattern within the moving bed reactor. Compared to multidimensional models, the 1-D model serves a practical purpose to help understand the reaction progress as well as to analyze the reactor design and operation. The 1-D model is computationally cost-effective and can be used for efficient sensitivity analysis. The three-interface shrinking core model is adapted in this reactive flow model to describe the overall conversion in the reactor. The assumptions in this model are given as follows:

a. Uniform temperature within the solid particles.
b. Both gas and solid streams in plug flow.
c. Three-interface unreacted shirking core model representing reaction kinetics.
d. Ignoring the temperature difference between gas and solid.

Assumptions (a) and (d) are valid because the heat of reaction in the three reactions in the SCL reducer is near zero. In addition, the bench-scale unit has an accurate external heating control system to ensure a uniform and isothermal temperature distribution across the bed. The gas and solid flow patterns in the moving bed can be approximated using assumption (b) due to relative uniformity of the radial variation of the gas and solid velocities in the moving bed. The SCL reducer operates with a moderate gas flow rate in which the gas dispersion effect is small.

This model describes the startup of the reactor and unsteady generation of gases, the changing flow patterns, and the reaction kinetics in the system, which is different from the previous work of using a steady-state assumption.[20] The mass balance equations for the gas phase and the solid phase in the reducer can be expressed as follows in the Lagrangian framework

$$\frac{D\varepsilon C_i}{Dt}=\sum_l \upsilon_{li}\frac{3(1-\varepsilon)V_l}{r_p}, \tag{13}$$

$$\frac{DE_i}{Dt}=\sum_l \upsilon_{li}\frac{3(1-\varepsilon)V_l}{r_p}, \tag{14}$$

where C_i stands for the concentrations of gas species, such as H_2, CO, H_2O, CO_2, and E_i stands for the concentration of solids, such as Fe_2O_3, Fe_3O_4, Fe_xO ($x = 0.952$) and Fe. The righthand side terms of Eqs. 13 and 14 denote the rates of change of the concentrations from the chemical reactions between the gases and the solids. $\upsilon_{li}$is the stoichiometric coefficient for species i appearing in the lth reaction. For the reactant species, the stoichiometric coefficient has a negative value $\upsilon_{li} < 0$. On the other hand, for the products, the stoichiometric coefficient has a positive value $\upsilon_{li} > 0$. Here, the chemical reaction is the only factor that changes the concentrations of every species, which establishes the relationship that the substantial derivatives equal the righthand side terms. Since both the gas and solid streams are in plug flow (assumption (b)), Eqs. 13 and 14 in the 1-D Eulerian framework can be rewritten as

$$\frac{\partial \varepsilon C_i}{\partial t}=-U_i\frac{\partial \varepsilon C_i}{\partial z}+\sum_l \upsilon_{li}\frac{3(1-\varepsilon)V_l}{r_p}, \tag{15}$$

$$\frac{\partial E_i}{\partial t}=-Us_i\frac{\partial E_i}{\partial z}+\sum_l \upsilon_{li}\frac{3(1-\varepsilon)V_l}{r_p}, \tag{16}$$

where U_i and U_{Si} are velocities of the gases and solids, respectively, and z is the spatial coordinate that begins at the bottom of the reducer and ends at the top of the reducer. The mathematical model developed here includes both time derivative terms and convective terms. This can help obtain the whole evolution process of the reactive flow in the 1-D moving-bed reducer. It should be noted that $D()/Dt$ in Eqs. 13 and 14 are substantial derivatives, indicating the change rate of the concentration of every species as the species move in the reducer. In Eqs. 15 and 16, the substantial derivatives have been split into local time derivative terms and spatially convective terms in the 1-D Eulerian framework.

The commonly used mathematical model for a steady-state 1-D moving bed is written as follows[26,28]

$$\frac{dy}{dz}=\frac{6(1-\varepsilon)S(V_1+V_2+V_3)4\pi r_p^2}{\pi {d_p}^3 G}, \tag{17}$$

$$\frac{dR_i}{dz}=\frac{6(1-\varepsilon)SV_i 4\pi r_p^2}{\pi d_p^3 W d_{Oi}}. \tag{18}$$

The newly developed 1-D model reduces to the previously report model when the system reaches the steady state. The detailed proof is provided in Appendix A.

Experimental Setup for Model Validation

A set of TGA tests were conducted for validating the particle kinetics model. The composite Fe_2O_3 particles were prepared and synthesized in a similar manner as in the previous work of the authors.[8] The particle size is between 1.4–1.7 mm, which is suitable for solid flow in the moving bed reactor. A 50-mg batch of particles was placed in the TGA, which was reduced by 200 mL/min STP H_2 at 900°C. The mass fraction of Fe_2O_3 in the solids is 60%, and the density of the solids is 2.5 g/cm^3. The particle porosity ε', varies from 0.001 to 0.005, depending on the macroscopic and microscopic properties of individual particles. The property values for H_2 used in the calculation are given in Eqs. 19, 22), most of which had been used by Hara et al. in their investigation of temperature effects on iron oxide pellet reduction.[29] The equilibrium constants for CO and iron oxides are calculated from the equilibrium constants given for H_2 together with the constants for the water-gas shift reaction, and all three CO reaction rate constants are one-fifth of those for H_2, based on the literature.[26] It is noted that the reaction-rate constants can be different for pellets with different compositions and different microstructures

$$k_{fH_2}=0.3\,\mathrm{m/s} \tag{19}$$

$$\begin{aligned} K_{1H_2}&=\exp(362/T+10.32)\\ K_{2H_2}&=\exp(-8580/T+8.98)\\ K_{3H_2}&=\exp(-2070/T+1.3) \end{aligned} \tag{20}$$

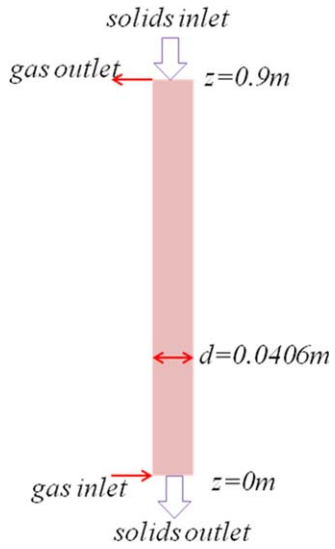

Figure 3. The schematic diagram of the moving-bed reducer.

[Color figure can be viewed in the online issue, which is available at wileyonlinelibrary.com.]

$$D_{1H_2}=0.13\times0.7516\varepsilon'(T/273)^{1.83}/10000$$
$$D_{2H_2}=0.20\times0.7516\varepsilon'(T/273)^{1.83}/10000 \quad (21)$$
$$D_{3H_2}=0.35\times0.7516\varepsilon'(T/273)^{1.83}/10000$$

$$k_{1H_2}=40\exp(-6650/T)$$
$$k_{2H_2}=80\exp(-8000/T) \quad (22)$$
$$k_{3H_2}=6800\exp(-14000/T)$$

A 2.5 kW_{th} bench-scale moving-bed reactor for conducting gas–solid reactions was constructed and operated in order to obtain the reactor performance data for modeling and scaling up analysis of the SCL process.[6] The length of the moving bed reactor is 0.9 m with an inner diameter of 0.0406 m, as shown in Figure 3. There is a number of gas and solid sampling ports along the reactor so that the fuel gas and oxygen carrier particle composition profiles in the reactor can be measured. Data from the bench-scale reducer study reported earlier by the authors were used to verify the 1-D reducer model.[6] The Fe_2O_3 particles, with similar properties as tested in the TGA experiments, were introduced at the top of the reducer at a feed rate of 12.87 g/min. The diameter of the solids is 4.0 mm, and the bed voidage of the reducer is 0.4. The pressure and the temperature of the system were 1 atm and 900°C, respectively. A simulated syngas was introduced from the bottom; the fractions of H_2, CO, CO_2, N_2 were 29.2, 43.8, 5.0 and 22.0%, respectively. The gas feed rate was 0.002262Nm^3/min.

Numerical Method

A FORTRAN90 program is coded based on the governing Eqs. 15 and 16, and the unreacted shrinking core kinetic model. For the temporal terms, a third-order TVD Runge-Kutta scheme is used for discretization.[30] For the spatial terms, a fifth-order WENO scheme is used.[31] The entire calculation procedure for reaction rates can be found in the work from Hara et al.[26] The initial conditions for the 1-D reducer modeling are that the bed is filled with Fe_2O_3 particles and the voidage is filled with syngas.

Results and Discussion

The 1-D dynamic model mainly consists of an individual oxygen carrier reaction kinetic model and a countercurrent, gas-solid flow model. For the kinetic modeling of individual oxygen carrier particles, key parameters include thermodynamic equilibrium constants K, reaction rate constants k_c, intraparticle diffusion coefficient D, and external mass transfer coefficient k_f. All the parameters have been considered in the unreacted shrinking core model, and have been validated by TGA experiments for determining the rate controlling step. The individual particle kinetic model is then integrated to the countercurrent flow model to simulate the moving-bed reducer. The 1-D reactor model is validated by the bench-scale experimental data, and sensitivity analyses are conducted to assess the importance of the model parameters. The effects of reactor length and feedstock ratio (G/W) are also evaluated to guide reactor design and operation.

Oxygen Carrier Kinetics

The three-interface USCM gives insight into how the overall reaction as well as the interfaces among Fe_2O_3, Fe_3O_4, Fe_xO and Fe migrates throughout the particle during the reduction process. To predict the conversions of the reactions conducted in a TGA, only Eq. 16 needs to be solved. Also, the spatial term in this equation vanishes since the pellets are stationary in the reducing environment. Figure 4 compares results between the oxygen carrier particle modeling and TGA experiments. The experimental curve is represented by 47 data points, which are calculated from 20 repeated experiments under the same conditions. The results show that the overall reaction progress predicted by the model is in favorable agreement with experimental data. Among all the three reduction reactions, Fe_2O_3 reduction is

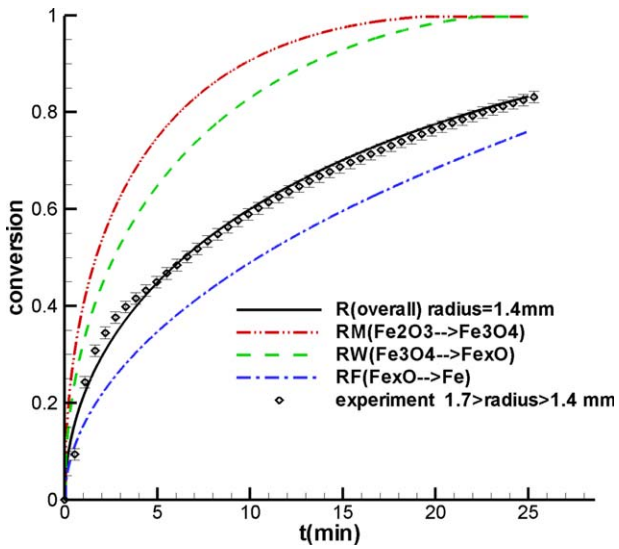

Figure 4. Comparison between TGA experimental results and USCM results for individual oxygen carrier particles reduction by hydrogen at 900°C.

[Color figure can be viewed in the online issue, which is available at wileyonlinelibrary.com.]

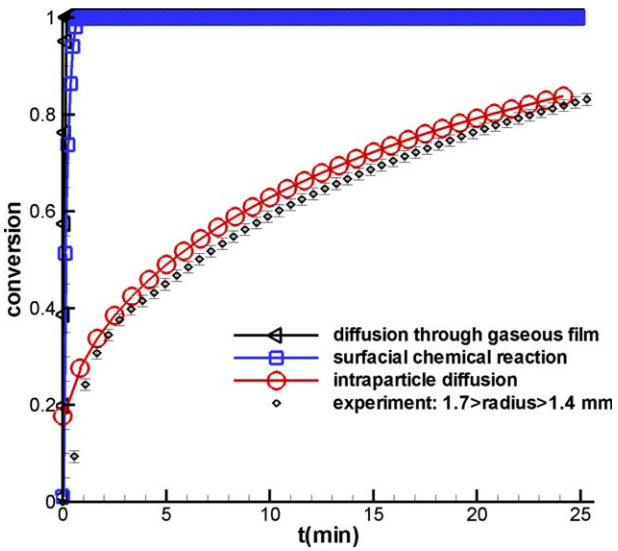

Figure 5. Reaction time for different controlling steps.

[Color figure can be viewed in the online issue, which is available at wileyonlinelibrary.com.]

the fastest, which is followed by Fe_3O_4 reduction. Near 22 min into the experiment, both reactions achieve full conversion, i.e., $R_M = R_W = 100\%$. The slowest reaction is wustite reduction to metallic iron, which only achieves 70% conversion ($R_F = 70\%$) at 22 min.

The USCM considers three factors influencing the reaction rate including external diffusion through gaseous film, intraparticle diffusion, and the surface chemical reaction. Reflected in the equations, k_f is the mass-transfer coefficient through gaseous film (cm/sec) and D is internal diffusivity in different iron oxide phases (cm^2/sec). For each surface reaction, k represents the reaction rate constant while K is the equilibrium constant. As shown in Figure 5, the USCM can help calculate the reaction time required by each step, and evaluate the importance of the three factors. The results show that the iron oxide particle reduction by hydrogen in this TGA study is dominated by intraparticle diffusion. It is noted that the gas environment in the TGA can be assumed to be pure hydrogen, which is different from the gas concentration and profile in the moving bed reducer. Thus, the intraparticle diffusion might not be the only rate controlling step in the moving bed operation. This will be further discussed in the following section. In general, the USCM can well represent the oxygen carrier reaction kinetics and, thus, will be embedded in the following 1-D reducer model.

Sensitivity Analysis of the Mathematical Model

This mathematical model for the moving-bed reducer incorporates a multitude of adaptable parameters. The sensitivity analysis of the model with respect to the variations in these parameters is performed to assess their significances. This study adopts the one-factor-at-a-time (OFAT) approach to investigate the effects of each parameter.[32] Comparing to absolute sensitivity, relative sensitivity is more effective for comparing parameters since it is measured by the dimensionless, normalized function.[33] The relative sensitivity of an arbitrary function F to the variation in a parameter α is defined as

$$S_\alpha^F = \frac{\partial F}{\partial \alpha}\bigg|_{(z,t)} \frac{\alpha_0}{F_0} = \frac{\Delta F/F}{\Delta \alpha/\alpha} \tag{23}$$

To simplify the sensitivity analysis in the moving-bed system, only the steady-state output at the bottom of the moving bed, i.e., $z = 0$, is monitored. The gas–solid feed rate ratio is fixed at 1.40 with the gas feed rate as 0.002262 Nm^3/min. The computed relative sensitivities of the fractional and overall solid conversions to variations in the adaptable parameters of this mathematical model are shown in Figure 6. It can be seen that the equilibrium constant of the third reaction K_{3H_2} is a dominant parameter. For the fractional solid conversions R_W and R_F, this parameter gives relative sensitivities that are more than one-order of magnitude larger than do other parameters. This suggests that other parameters do not have strong influence on the computed results.

It should be noted that, the relative sensitivities of the fractional solid conversion with respect to all parameters are negligibly small. This is not surprising since the equilibrium constant K_{1H_2} is several orders of magnitude larger than the other two equilibrium constants K_{2H_2} and K_{3H_2}at the operating temperature, $T = 1173$K (see Eq. 20), and this large K_{1H_2} ensures that R_M reaches nearly 100% at the current gas–solid feed rate ratio when all model parameters are varied within a practical range. In the simulations, the moving-bed reducer is adequately long to fully convert the introduced syngas at the given gas–solid feed rate ratio. As a result, the variations of all model parameters will not change the fact that the syngas are nearly fully converted and the outlet solid conversion can be readily determined from the mass conservation. This explains why the relative sensitivities of the overall solid conversion R are small and almost identical with respect to all parameters. As the overall solid conversion is calculated as a weighted sum of the three fractional conversions, a much higher sensitivity of the model with respect to K_{1H_2} might be expected. However, it can be found in Figure 6 that the relative sensitivities of R_W and R_F have opposite signs with respect to K_{1H_2}. Most of the changes in R_W and R_F are cancelled when the weighted sum to obtain R is executed. Thus, K_{1H_2} is not of significant relevance to R even it does influence R_W and R_F in a much stronger way.

It is worth to mention that, the relative sensitivities with respect to the parameters, K_{1H_2}, $k_{1H_2}k_{2H_2}$, D_{1H_2} and k_{fH_2} are

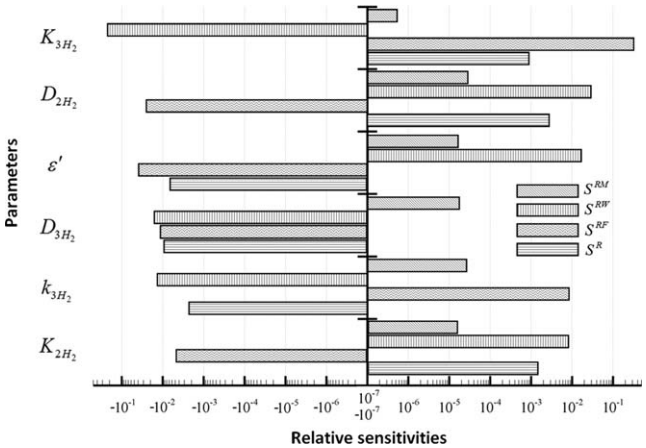

Figure 6. The relative sensitivities of the fractional solid conversions R_M, R_W, R_F and the overall solid conversion R to variations in the parameters of the mathematical model.

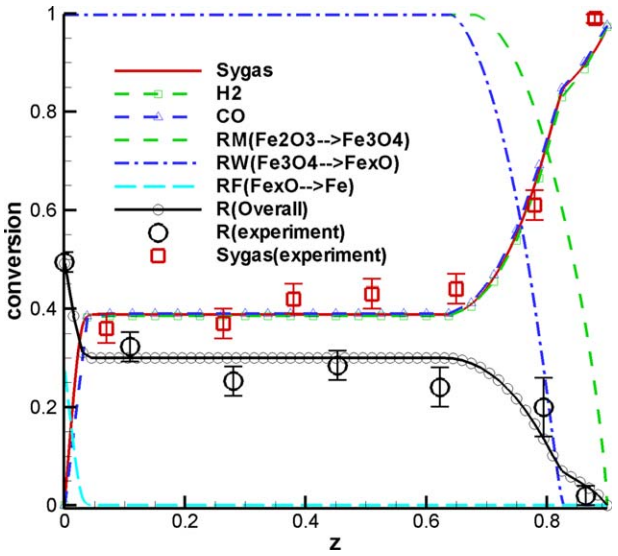

Figure 7. The comparison of the gases and solids conversions between the numerical results and the previous experimental data in the moving-bed reducer 6.

[Color figure can be viewed in the online issue, which is available at wileyonlinelibrary.com.]

negligibly small, less than 0.001, and, thus, are not shown in Figure 6.

1-D Moving-Bed Reducer at Steady State

In the SCL system, the moving-bed reducer is designed to fully convert the syngas to CO_2 and H_2O at the top of the moving-bed reducer. At the same time, a maximum oxygen carrier conversion should be obtained at the bottom of the reducer. In order to verify the 1-D reducer model, the previous bench-scale reducer testing is used to specify the model input and output. Figure 7 illustrates the numerical results as well as the experimental results of the moving-bed reducer when steady state is reached. The error bars on the experimental symbols represent the standard variations from eight repeated experiments. The steady-state numerical results show that the syngas conversion at top of the reducer is 97.5% at the top, while the oxygen carrier conversion is 49.2% at the bottom. In the bench-scale experiment, a syngas conversion in excess of 99.5% and an oxygen carrier conversion of nearly 50% were obtained. It is noted that, the number of the experimental data points is not large enough to form continuous lines. This is because it is not desirable to fabricate many ports along the moving-bed reactor for operation under such a high temperature. Still, it can be seen that all the experimental data points stay around the simulated lines, which further validates the 1-D mathematical model. Therefore, this 1-D model can be used for further investigations of the reducer in the bench-scale SCL system.

The 1-D reducer model can not only calculate the overall gas and solid conversions at the reactor outlets, but can also provide dynamic gas and solid conversion profiles inside the reactor, which is helpful for understanding the reaction behavior. As shown in Figure 7, the calculated syngas and oxygen carrier conversion profiles along the axial locations of the reactor at steady state conditions match well with the previous profiles measured from sampling ports. Both experimental and modeling results show that the gas and solid conversion profiles have opposite trends because of the countercurrent contact pattern. The results also indicate that the conversion rates at both ends are much faster than the conversion rates in the middle section of the reducer. The syngas and Fe_2O_3 particles are introduced at the bottom and the top of the reducer, respectively, which creates a large driving force for reduction reaction going forward. In the middle section, however, the gas and solid compositions are close to an equilibrium state, and, thus, nearly no reaction is observed. Specifically, the modeling results show that the equilibrium state is maintained when the gas and solid conversions are 38 and 30% (pure $Fe_{0.952}O$), respectively. Such an intermediate equilibrium stage and overall gas and solid conversions can be also predicted by a multistage equilibrium model developed in a preceding work.[6] Both the equilibrium model and the kinetic model have been validated by experimental data, and both modeling results show that the countercurrent moving-bed reducer design is capable of ensuring a full syngas conversion while enhancing oxygen carrier conversion.

As shown in Figure 7, under the current operation condition and reducer design, an individual particle quickly completes the reduction from Fe_2O_3 to Fe_3O_4 and then to Fe_xO at the top. The reduction from Fe_xO to Fe is then limited by thermodynamic equilibrium before the gas profile is changed at the bottom where fresh syngas is introduced. Compared with the previous oxygen carrier kinetic studies in the TGA where only intraparticle diffusion dominates the reduction process, the oxygen carrier particle reduction in the moving-bed reducer is restricted by the reaction thermodynamics. It is also noted in Figure 7 that there is a minor difference between the modeling results and experimental data. Such deviation may result from the flow and temperature maldistribution across the bed and from the randomness of the gas and solid sampling in the experiments. The unsaturation degree x in the wustite (Fe_xO) phase varies from $0.830<x<0.952$, which could also affect the equilibrium conditions, and, thus, compositions of the system.

1-D Moving-Bed Reducer at Unsteady State

A startup process is simulated in this scenario. The bed is initially filled with Fe_2O_3 particle and syngas, which is consistent with the typical startup procedure in the bench scale experiment. As stated in the section Mathematical Model, the temporal terms are considered in the governing equations of the reducer system. This means that not only can the steady state of the reducer be revealed by the simulation, but the dynamic, unsteady state conversion profiles can also be modeled. Figure 8 displays the conversion profiles of both the solids and the gases at different times under unsteady-state conditions. The experimental data of the gas conversion from one port are also shown in the early stages of the experiment. It can be seen that these data are close to, but slightly smaller than the simulated results. This deviation can be attributed by the gas–solid feed-rate ratio effects, which is discussed in the Reducer Operation section. During the early stages, the conversion profiles change rapidly (see the results at t = 1,000 s in Figure 8a). The major pattern of the conversion profiles has formed at the bottom of the reducer when $t = 5{,}000$ s (see Figure 8b). This time is about one residence time for the solid oxygen carrier particle, which is consistent with the typical time observed for the

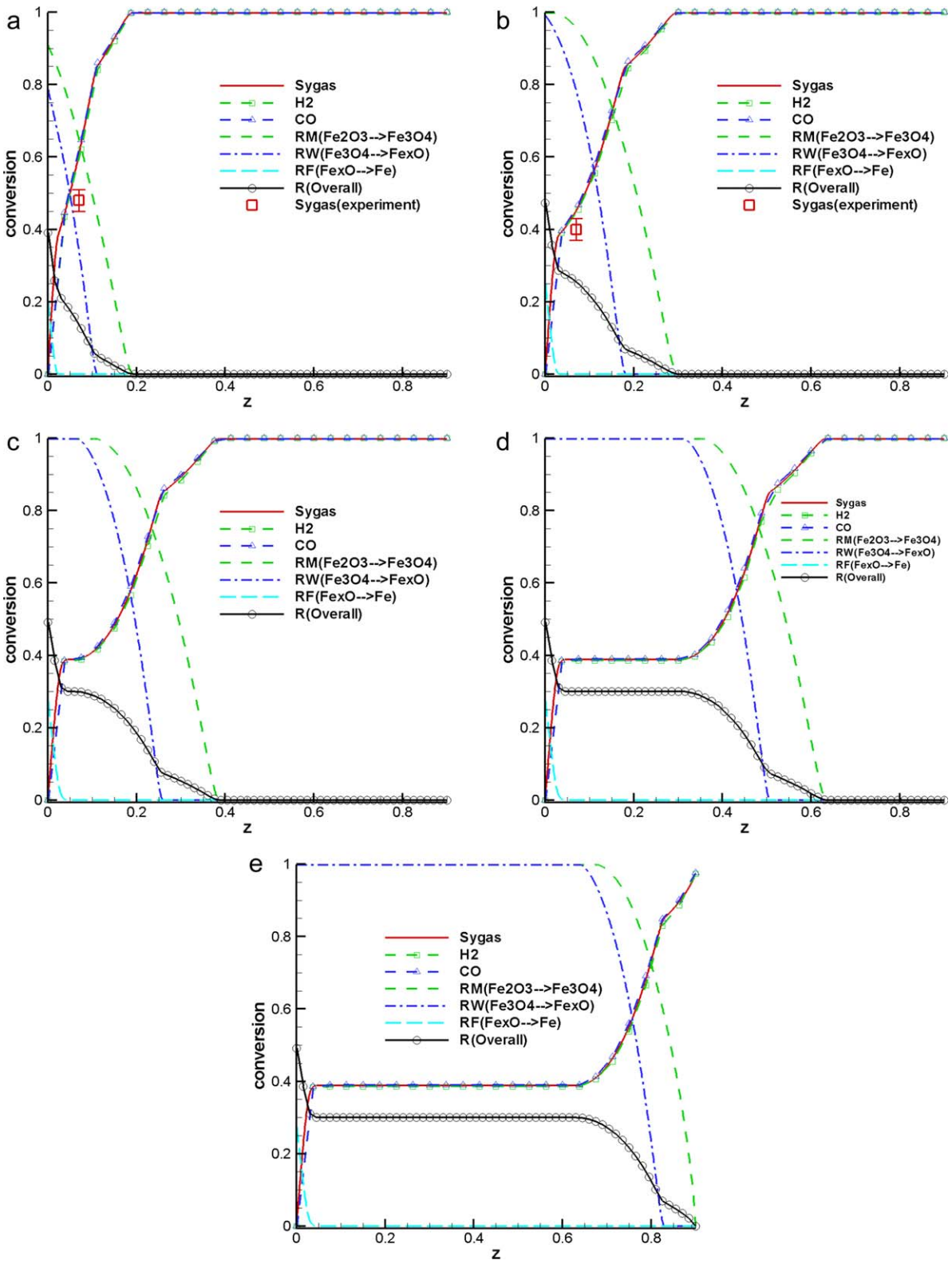

Figure 8. The conversion profiles of both gases and solids at different times in the reducer.

(a) $t = 1{,}000$ s, (b) $t = 5{,}000$ s, (c) $t = 20{,}000$ s, (d) $t = 80{,}000$ s, and (e) $t = 150{,}000$ s. [Color figure can be viewed in the online issue, which is available at wileyonlinelibrary.com.]

syngas to be fully converted at the reducer gas outlet in the bench scale test. Subsequently, as shown in Figure 8c and 8d, the rightmost segments correspond to the first two reduction reactions (Fe_2O_3-Fe_3O_4-Fe_xO), and move toward the top of the reducer without significant shape change, while the leftmost segments correspond to the third reaction (Fe_xO—Fe) and stay at the bottom of the reducer. The equilibrium stage emerges between the left and right segments,

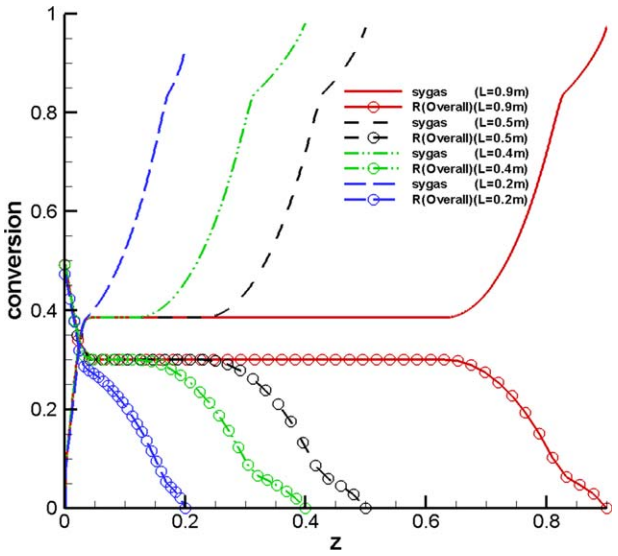

Figure 9. The steady overall conversion profiles of syngas and solids when the reducer is shortened.

[Color figure can be viewed in the online issue, which is available at wileyonlinelibrary.com.]

and extends as reaction progresses. The system reaches its steady state around 150,000 s (see Figure 8e), which is caused by the slow translational movement of the profiles toward the top of the reducer.

From the observation of the numerical results, two aspects arise and will be discussed later. The first aspect is that since the conversion profile is mostly flat in the middle part of the reducer, the reducer may be shortened without affecting the reactions inside. The second aspect is that the efficiency of the current case is relatively low. The system takes too long a time to reach the steady state because of the thermodynamic equilibrium stage formation in the middle part of the reducer. Adjustment of the feed-rate ratio between the gases and solids may be a simple and straightforward way to decrease the time needed to for the system to achieve a steady state. Note, for convenience, the time needed to achieve a steady state is also called the converging time in the remainder of this article. It is not used in the context of simulation time, only in the time to reach actual the steady state in reactor time.

Reducer Design: Effective Reducer Length

The reducer length can be optimized using the 1-D moving-bed model. Reducers with lengths of 0.5 m, 0.4 m and 0.2 m are simulated under the same initial and boundary conditions as are the simulations in the section 1-D Moving-Bed Reducer at Steady State. The steady-state simulation results are shown in Figure 9, from which it can be seen that the conversion profiles of the reducers with the length of 0.5 m and 0.4 m have approximately the same conversion profiles as the reducer of length 0.9 m. The main difference is that the flat parts or the equilibrium state of the profiles in the shorter reducers are shortened. However, the reducer with 0.2 m length seems to be too short to complete the reactions, unlike the other cases. The flat, equilibrium parts of the profiles in the reducer of 0.2 m have almost completely disappeared. As a result, the syngas conversion in this case is not as high as the conversion in the reducers with longer lengths. A reducer of 0.4 m can achieve exactly the same results as a reducer of 0.9 m, indicating that the design of the current reducer is conservative and the reducer can be shortened without changing the reaction processes.

It is noted that no matter how long the reducer is designed, the segments with solid conversion higher than 30% are always present at the bottom of the reducer. Under the given syngas to oxygen carrier flow rate ratio, the reducing gas is almost completely converted at the top, and the reducing gas concentration at the middle and top sections is not enough to drive the reaction equilibrium toward wustite reduction to metallic iron. Under this circumstance, the high-reducing gas concentration can only be reached near the bottom of the reducer where the new reducing gases are just injected in.

It should be also noted that the conversion profiles with the plateau are not a trivial superposition of the effects of feeding fresh solid and gases from the two ends of the reactor. They do not appear at all gas to solid ratios even when the reactor is adequately long. Only when the gas to solid ratio is larger than a certain critical value, can the profiles associated with the reactions $Fe_2O_3 \rightarrow Fe_3O_4$ and $Fe_3O_4 \rightarrow Fe_xO$ move toward the top of the reducer. This is because the unreacted reducing gas from the bottom can reduce the Fe_2O_3 coming from the top to Fe_xO but cannot subsequently reduce the newly generated Fe_xO to Fe due to the limitation of the reaction equilibrium. Therefore, the reducing gas and the Fe_xO coexist in the middle part of the conversion profiles. This coexistence forms the plateau in the conversion profiles. To further describe the mechanism of the formation of the plateau, the effect of the gas–solid feed-rate ratio is elaborated in the next section.

Reducer Operation: Gas–solid Feed Rate Ratio Effect

The gas–solid feed-rate ratio is an important variable in the moving-bed reducer operation. Since considerable time is required for the system to reach the steady state in the previous scenario, it is desired to determine how the converging time varies with the feed rate ratio. Before further numerical simulations are conducted, an analysis based on the equilibrium constants of the three reduction reactions is performed. The equilibrium constant of the third reaction is $K_3 = 0.6283$ at 900°C. When the syngas can be fully converted in the reducer, the ideal percentage of the syngas consumed in the first and second reactions would be $1/(K_3 + 1) = 61.414\%$ with the rest of the syngas (38.586%) being consumed in the third reaction. As illustrated above, Fe_2O_3 in the solids can be converted completely into Fe_xO by the first and second reactions. The generated Fe_xO can only be partially converted into Fe from the lack of reducing gas. The total amount of Fe_2O_3 is determined by the 61.414% of the reducing gases. The amount of converted Fe_xO corresponds to the 38.586% of the reducing gases. Through the combination of the first two reactions

$$\frac{x}{3x-2}Fe_2O_3 + H_2/CO \leftrightarrow H_2O/CO_2 + \frac{2}{3x-2}Fe_xO, \quad (24)$$

and the third reaction

$$Fe_xO + H_2/CO \leftrightarrow H_2O/CO_2 + xFe, \quad (25)$$

the feed rate ratio between gas and solids can be determined to be 1.4647 when the reducing gases are critically and fully

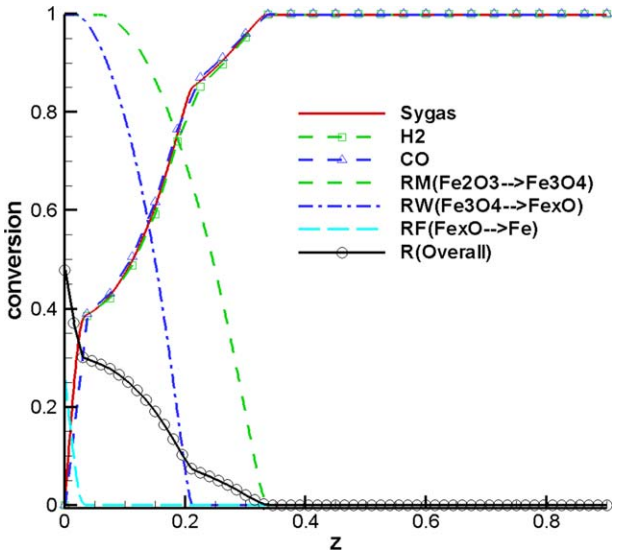

Figure 10. The conversion profiles when the solids feed rate increases by 5%.

This lower solids feed rate makes the feed rate ratio between gases and solids decrease to 1.4538, lower than the critical ratio 1.4647. [Color figure can be viewed in the online issue, which is available at wileyonlinelibrary.com.]

converted. At this critical ratio of 1.4647, a maximized solids conversion of 48.823% can be obtained to ensure a full syngas conversion at the top of the reducer.

From the data of previous experiments,[6] the feed rate ratio between gas and solids is found to be 1.5265, which is slightly higher than the critical ratio of 1.4647. In the following numerical investigation, the gas feed rate remains unchanged, and the solids feed-rate is changed to adjust the feed rate ratio between gas and solids. The situation with a ratio lower than the critical value is first examined. The solids feed rate is increased by 5%, making the gas–solid feed rate ratio decrease to 1.4538. The results of this case are shown in Figure 10, and the steady-state conversion profiles are significantly different from the previous results. All the profiles appear near the bottom of the reducer with an unreacted zone at the top. The converging time of this case is about 20,000 s, which is much less than that of the case with a feed-rate ratio of 1.5265. This profound difference can be understood easily as follows. After the case with the ratio of 1.4538 reaches the steady state, imagine how the conversion profiles would change if the feed rate ratio is increased to 1.5265. Because the system can only fully convert the gases when the feed-rate ratio is lower than the critical value 1.4647, the system now cannot fully convert all of the fuel gases. Therefore, the excessive reducing gases will keep going upward beyond the position of $z = 0.35$ (see Figure 10) and will react with the unreacted Fe_2O_3 in the upper positions, making the entire profiles except the bottom segment moving slowly toward the top of the reducer. The moving speed of the profiles is determined by the amount of the excessive reducing gases and is, thus, essentially determined by the feed rate ratio. The salient changes of the profiles during this movement are that the middle segments of the profiles keep expanding (one can refer to Figure 8b–e for better understanding). The expansion of the middle segments is because an equilibrium stage is reached in that area

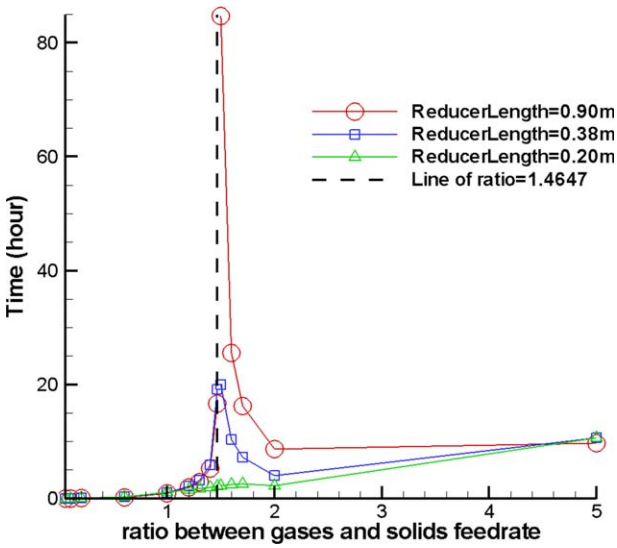

Figure 11. The converging time verse the feed rate ratio between gases and solids.

[Color figure can be viewed in the online issue, which is available at wileyonlinelibrary.com.]

because of the excess reducing gases. It can be conjectured that when the feed-ratio is only slightly higher than the critical ratio, the converging time would be extremely long since the unsteady movement of the profile are very slow. As the result, such gas to solid feed rate ratio should be avoided in a practical reducer operation.

Generally, the converging time can be shortened in two ways. One is to make the feed-rate ratio slightly smaller than the critical ratio. The other is to shorten the reducer to a proper size without affecting the reactions inside. A series of numerical simulations with different feed-rate ratios and reducer lengths is performed. Figure 11 shows that the converging time varies as the feed-rate ratio between the gas and solids is changed. The converging time is prohibitively long when the feed ratio is close to but higher than the

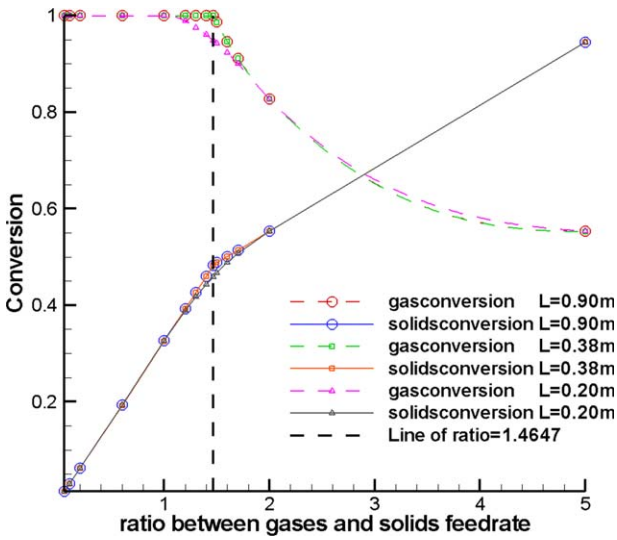

Figure 12. The gases and solids conversions vs. the feed rate ratio between gases and solids.

[Color figure can be viewed in the online issue, which is available at wileyonlinelibrary.com.]

critical ratio. For the actual moving-bed operation, a ratio slightly below the critical ratio is recommended. However, if the ratio is too small, this operation is not favorable since the conversion of the solids becomes low, which requires a large oxygen carrier circulation rate. It is also noticed from Figure 11 that a shorter reducer needs less time to reach the steady state. Figure 12 displays the evolution of the gas and solids conversion profiles as the feed rate ratio varies. On one hand, the gas conversion cannot reach 100% after the feed rate ratio goes beyond the critical value. On the other hand, the reducer with a length of 0.2 m is not long enough to function as well as the other longer reducers since the gas conversion is appreciably lower than 100% even when the feed ratio is lower than the critical value. Nevertheless, the reducer of 0.38 m actually functions as well as the one of 0.9 m, indicating the shorter reducer can be considered as a practical reducer design.

Conclusions

The SCL process circulates iron-based oxygen carrier particles through three reactors, namely the reducer, the oxidizer, and the combustor, to perform reduction-oxidation reaction cycles for carbon dioxide capture and hydrogen production from coal or biomass derived syngas. The countercurrent moving-bed operation of the reducer highlights the SCL technology. This article presents a 1-D flow model for moving-bed reducer in SCL system. The three-interface unreacted shrinking core model is applied to describe the reaction of the gas and solid flows within the reactor. The code is validated through comparing the simulated results with experimental data. The 1-D model gives a good understanding of the actual reaction properties in the moving-bed reducer. In this study, the entire progress of the composition evolution in the moving-bed reducer is obtained through explicit temporal integration. Second, a shorter reducer is suggested based on the numerical simulations on reducers with different lengths. Third, the converging time before the reducer reaches the steady state is analyzed by varying the ratio between the gas and solids feed rates. The results conclude that a minor change of the feed-rate ratio could cause significant differences in the converging time. Specifically, there are two general ways to shorten the time for the system to reach the steady state: one is to make the feed-ratio slightly smaller than the critical ratio, and the other is to shorten the reducer to a proper size without affecting the reactions inside the reactor. Thus, 1-D moving-bed reactor model effectively provides a practical strategy in optimizing the reducer design and operation in the SCL process.

Acknowledgment

This work was sponsored by the U.S. Dept. of Energy National Energy Technology Laboratory's University Coal Research Program (Project DE-NT0007428). The authors would like to acknowledge the valuable input from Dr. Zhao Yu and Mr. Omar McGiveron during the preparation of this article.

Notation

ε = voidage of the bed
ε' = porosity of particles
C = concentration of reducing gas
D = diffusion coefficient of reducing gas
d = reactor diameter
d_O = initial content of reducible oxygen atom in the pellet
d_p = pellet diameter
G = molar flow rate of gas
K = equilibrium constant
k_c = reaction-rate constant
k_f = mass-transfer coefficient through gaseous film
P = pressure
Q = gas-flow rate
R = fractional reduction
$\tilde{R}$ = gas constant
r_p = pellet radius
S = cross-sectional area of reaction tube
S_α^F = relative sensitivity of F to the variation in a parameter α
T = temperature
t_c = time needed for the moving bed to reach the steady state
V = reaction rate
W = federate of pellets
y = molar fraction of reducing gas
y_i^* = equilibrium molar fraction of reducing gas for the ith step reaction
z = distance from bottom of the bed

Subscripts

M(or 1) = chemical reaction from Fe_2O_3 to Fe_3O_4
W(or 2) = chemical reaction from Fe_3O_4 to Fe_xO
F(or 3) = chemical reaction from Fe_xO to Fe

Literature Cited

1. Figueroa JD, Fout T, Plasynski S, McIlvried H, Srivastava RD. Advances in CO_2 capture technology-The U.S. Department of Energy's carbon sequestration program. *Int J Greenhouse Gas Control*. 2008;2:9–20.
2. Li F, Fan L.-S. Clean coal conversion processes-progress and challenges. *Energy Environ Sci*. 2008;1:248–267.
3. Connell DP, Dunkerley ML. Systems Analysis of the Coal Direct Chemical Looping Process for Coal-Based Electricity Production with *in situ* Carbon Dioxide Capture. In 36th International Technical Conference on Clean Coal and Fuel Systems: Proceedings, Clearwater, FL, June 5–9, 2011.
4. Fan L.-S, Zeng L, Wang W, Luo S. Chemical looping processes for CO_2 capture and carbonaceous fuel conversion-prospect and opportunity. *Energy Environ Sci*. 2012;5:7254–7280.
5. Lyngfelt A. Oxygen carriers for chemical-looping combustion-4000 h of operational experience. *Oil Gas Sci Technol*. 2011;66;161–172.
6. Li F, Zeng L, Velazquez-Vargas, LG, Yoscovits Z, Fan L.-S. Syngas chemical looping gasification process: bench scale studies and reactor simulations. *AIChE J*. 2010;56:2186–2199.
7. Mattisson T, Johansson M, Lyngfelt A. Multicycle reduction and oxidation of different types of iron oxide particles - application to chemical-looping combustion. *Energ Fuel* 2004;18:628–637.
8. Li F, Kim H, Sridhar D, Wang F, Zeng L, Fan L.-S. Syngas chemical looping gasification process: oxygen carrier particle selection and performance. *Energy Fuels*. 2009; 23:4182–4189.
9. Lyngfelt A, Thunman H. In: Thomas DC, Benson S, eds. *Capture and Separation of Carbon Dioxide from Combustion Sources; Carbon Dioxide Capture for Storage in Deep Geologic Formations-Results from the CO_2 Capture Project*. 1st ed. Oxford, UK: Elsevier; 2005;1.chap 36.
10. Shen L, Wu J, Xiao J. Experiments on chemical looping combustion of coal with a NiO based oxygen carrier. *Combust Flame*. 2009;156: 721–728.
11. De Diego L, García-Labiano F, Gayán P, Celaya J, Palacios J, Adanez J. Operation of a 10 kWth chemical-looping combustor during 200 h with a CuO-Al2O3 oxygen carrier. *Fuel*. 2007;86:1036–1045.
12. Pröll T, Kolbitsch P, Bolhàr-Nordenkampf J, Hofbauer H. A novel dual circulating fluidized bed system for chemical looping processes. *AIChE J*. 2009;55:3255–3266.
13. Ryu H-J, Jo S-H, Park Y-C, Bae D-H, Kim S. Long term operation experience in a 50 kWth chemical looping combustor using natural gas and syngas as fuels. In 1st International Conference on Chemical Looping: Proceedings, 2010, IFP-Lyon, France, March 17–19, 2010.
14. Sridhar D, Tong A, Kim HR, Zeng L, Li F, Fan L.-S. Syngas chemical looping process: Design and construction of a 25kWth sub-pilot unit. *Energy Fuels*. 2012;26(4):2292–2302.

15. Tong A, Sridhar D, Sun Z, Kim HR, Zeng L, Wang F, Wang D, Kathe M, Luo S, Sun Y, Fan L.-S. Continuous high purity hydrogen generation from a syngas chemical looping 25kwth sub-pilot unit with 100% carbon capture. *Fuel*. 2012; In Press.
16. Kasten PR, Amundson NR. Analytical Solution for Simple Systems in Moving Bed Adsorbers. *Ind Eng Chem*. 1952;44(7):1704–1711.
17. Amundson NR. Solid-Fluid Interactions in Fixed and Moving Beds Fixed Beds with Small Particles. *Ind Eng Chem*. 1956;48 (1): 26–35.
18. Amundson NR, Arri LE. Char gasification in a countercurrent reactor. *AICHE J*. 1978;24(1):87–101.
19. Adanez J, Abad A, Garcia-Labiano F, Gayan P, de Diego LF. Progress in Chemical-Looping Combustion and Reforming technologies. *Progr Energ Comb Sci*. 2012;38:215–282.
20. Kang K-S, Kim C-H, BAE K-K, CHO W-C, Jeong S-U, Kim S-H, Park C-S. Modeling a counter-current moving bed for fuel and steam reactors in the TRCL process. *Int J Hydrogen Energ*. 2012;37(4): 3251–3260.
21. Turkdogan ET, McKewan WM, Zwell L. Rate of oxidation of iron to Wustite in water-hydrogen gas mixtures. *J Phys Chem*. 1965;69: 327–334.
22. Turkdogan ET, Vinters JV. Gaseous reduction of iron oxides: Part I. Reduction of hematite in hydrogen. *Metall Trans*. 1971;2(11):3175–3188.
23. Turkdogan ET, Vinters JV. Gaseous reduction of iron oxides. *Metall Trans*. 1972;3(6):1561–1574.
24. Hossain MM, de Lasa HI. Chemical-looping combustion (CLC) for inherent CO2 separations-a review. *Chem Eng Sci*. 2008;63:4433–4451.
25. Levenspiel O. *Chemical Reaction Engineering*. 3rd ed. New York: John Wiley & Sons, Inc.; 1998.
26. Hara Y, Sakawa M, Kondo S. Mathematical model of the shaft furnace for reduction of iron ore pellet. *Tetsu-to-Hagane*. 1976;62:315–323.
27. Negri ED, Alfano OM, Chiovetta MG. Direct reduction of hematite in a moving-bed reactor. analysis of the water gas shift reaction effects on the reactor behavior. *Ind Eng Chem Res*. 1991;30:474–482.
28. Yanagiya T, Yagi J, Omori Y. reduction of iron oxide pellets in moving bed. *Ironmaking Steelmaking*. 1979;3:93–100.
29. Hara Y, Tsuchiya M, Kondo S. Intraparticle temperature of iron-oxide pellet during the reduction. *Iron Steel Inst Japn*. 1974;60(9): 1261–1270.
30. Shu CW and Osher S. Efficient implementation of essentially non-oscillatory shock-capturing schemes, II. *J Comp Phy*. 1989;83:32–78.
31. Jiang GS, Shu CW. Efficient implementation of weighted ENO schemes. *J Comp Phy*. 1996;126:202–228.
32. Saltelli A, Annoni P. How to avoid a perfunctory sensitivity analysis. *Environ Model Software* 2010;25:1508–1517.
33. Smith ED, Szidarovszky F, Karnavas WJ. and Bahill AT. Sensitivity analysis, a powerful system validation technique. *Open Cybernetics Systemics J*. 2008;2:39–56.

Appendix A

We will prove that the aforementioned Eqs. 15 and 16 and Eqs. 17 and 18 are basically equivalent.

Assume that C_i in Eq. 15 stands for H_2. Dividing Eq. 15 by εC_o, we will obtain

$$\frac{\partial y_{H_2}}{\partial t} = -U_i \frac{\partial y_{H_2}}{\partial x_i} + \sum_l \upsilon_{li} \frac{3(1-\varepsilon)V_l}{r_p \varepsilon C_o} \tag{A1}$$

It can be shown that

$$\frac{6V_i 4\pi {r_p}^2}{\pi {d_p}^3} = \frac{3V_i}{r_p}.$$

since $d_p = 2r_p$.

For steady-state problems, the term of time derivative would vanish, and Eq. A1 will reduce to

$$\frac{dy_{H_2}}{dx_i} = \sum_l \upsilon_{li} \frac{3(1-\varepsilon)V_l}{U_i r_p \varepsilon C_o} \tag{A2}$$

For H_2, the stoichiometric coefficient is 1. So we only need to show that

$$\frac{S}{G} = \frac{1}{U_i \varepsilon C_o}, \tag{A3}$$

where, G is the gas feed rate, S is the cross section area of the reducer, U_i is the gas velocity in the reducer, and εC_o is the equivalent concentration of H_2. Note, C_o is the superficial concentration of H_2 and ε is the voidage of the moving bed. From the definition of the variables in Eq. A3 we know this equation holds true. Now, the equivalence between Eqs. 15 and 17 is approved.

Similarly, we can demonstrate that Eqs. 16 and 18 are equivalent. In order to show the equivalency, we want to demonstrate first the following equation holds

$$\frac{S}{W d_{Oi}} = \frac{\upsilon_{li}}{U s_i E_0}, \tag{A4}$$

where E_0 is the initial concentration of Fe_2O_3; W is the feed rate of the pellet; and d_{Oi} is the initial concentration of the reducible oxygen in hematite, magnetite or wustite. If i denotes Fe_2O_3, the value of d_{Oi} is $1/3$ of that of Fe_2O_3 because only one oxygen atom can be reduced in every three Fe_2O_3 molecular (see the reaction formula in which the reaction between Fe_2O_3 and CO or H_2 is 3:1). Also, we know that the stoichiometric coefficient υ_{li} of the first reaction is 3. We can see Eq. A4 holds through the explanation given earlier.

It should be noted that each equation in Eq. 18 is actually a sum of several equations of Eq. 16 because of the definition of the fractional reductions. One will find that Eqs. 16 and 18 are indeed equivalent after performing the simple summation.

Manuscript received Oct. 22, 2012, and revision received Jun. 14, 2013.